Structure and dynamics of pentacene on SiO_2: From monolayer to bulk structure

Aldo Brillante,* Ivano Bilotti, Raffaele Guido Della Valle, and Elisabetta Venuti
Dipartimento di Chimica Fisica e Inorganica and INSTM-UdR Bologna, and Università di Bologna, Viale Risorgimento 4, I-40136 Bologna, Italy

Alberto Girlando and Matteo Masino
Dipartimento di Chimica GIAF and INSTM-UdR Parma, and Università di Parma, Parco Area delle Scienze, I-43100, Parma, Italy

Fabiola Liscio and Silvia Milita
CNR-IMM, Istituto per la Microelettronica e Microsistemi, Via P. Gobetti 101, I-40129 Bologna, Italy

Cristiano Albonetti, Pasquale D'angelo, Arian Shehu, and Fabio Biscarini
CNR-ISMN, Istituto per lo Studio dei Materiali Nanostrutturati, Via P. Gobetti 101, I-40129 Bologna, Italy
(Received 29 March 2012; published 8 May 2012)

We have used confocal micro Raman spectroscopy, atomic force microscopy (AFM), and x-ray diffraction (XRD) to investigate pentacene films obtained by vacuum deposition on SiO_2 substrates. These methods allow us to follow the evolution of lattice structure, vibrational dynamics, and crystal morphology during the growth from monolayer, to TF, and, finally, to bulk crystal. The Raman measurements, supported by the AFM and XRD data, indicate that the film morphology depends on the deposition rate. High deposition rates yield two-dimensional nucleation and quasi-layer-by-layer growth of the T-F form only. Low rates yield three-dimensional nucleation and growth, with phase mixing occurring in sufficiently thick films, where the T-F form is accompanied by the "high-temperature" bulk phase. Our general findings are consistent with those of previous work. However, the Raman measurements, supported by lattice dynamics calculations, provide additional insight into the nature of the TFs, showing that their characteristic spectra originate from a loss of dynamical correlation between adjacent layers.

DOI: 10.1103/PhysRevB.85.195308 PACS number(s): 81.05.Fb, 78.30.Jw, 68.37.Ps, 63.22.Np

I. INTRODUCTION

Pentacene is nowadays considered one of the most promising candidates for plastic electronics,[1] since thin films (TFs) obtained by ultrahigh-vacuum deposition display excellent charge transport characteristics. On the other hand, charge carrier mobility is crucially dependent on the crystallinity of films, i.e., grain size, polymorphism, and defects, so that a large number of studies have been devoted to the characterization and possible improvement of pentacene TF growth. As a matter of fact, even the simple structural characterization of pentacene crystals and films has proven to be rather challenging, in view of the occurrence of several, slightly different polymorphs. All the known pentacene bulk crystal[2–5] and TF structures on amorphous SiO_2 substrates[5–12] indeed share a similar molecular packing. All structures are triclinic, with space group $P\bar{1}$ and two inequivalent molecules in the unit cell ($Z = 2$). The two molecules are twisted with respect to each other in the characteristic "herringbone" arrangement and sit on layers parallel to the (001) plane.[2,5,13]

In all cases, the pentacene molecules stand approximately normal to the most developed crystal face or to the TF layer, so that the interplanar distance $d(001)$, which describes the layer spacing, is the largest periodic distance. This parameter cannot provide complete information on the phase but still allows for its quick identification.[14] In the films four d spacings have been identified by x-ray techniques: 14.1, 14.4, 15.1, and 15.4 Å.[6–8,15] The first two values correspond to those of the low-temperature (LT) and high-temperature (HT) bulk phases,[2–5] while the interplanar distances of 15.1 and 15.4 Å belong to genuine TF forms. The one having $d(001) = 15.4$ Å[10,11,16] is the most commonly encountered and is also found in ultra-TFs[16,17] and monolayers (MLs).[8,18] In films the layers always lie parallel to the interphase, since the (001) surface exhibits the lowest surface energy.[19,20]

The most remarkable thing, however, is that 100-nm-thick films display the same TF lattice constants as ultra-TFs,[16] so that the films share the same structure regardless of the thickness and in regimes for which only bulk structures would be expected. Depending on the growth conditions, films may also show phase mixing, with the TF form accompanied by the HT bulk phase,[6,9,14,16] which may even nucleate as early as the first ML.[21] Experimental[16,22] and theoretical[20] works have shown that the film morphology may be controlled by tuning the growth parameters, in particular, the deposition rate Φ. Low deposition rates yield three-dimensional (3D) nucleation and growth, leading to ill-connected grains, whereas high rates yield 2D nucleation and quasi-layer-by-layer growth, leading to continuous films suitable for charge transport.[20,22]

The aim of the present work is to study the evolution of the crystalline structure of pentacene films during the growth from monolayer, to TF, and, finally, to bulk crystal, by confocal micro Raman spectroscopy[23,24] accompanied by morphological characterization via atomic force microscopy (AFM) and by verification of the crystallographic phase by x-ray diffraction (XRD). Although not widely used for this purpose, the spectroscopic technique is an effective, prompt,

and reliable method of phase identification, with a very high sensitivity to structural and morphological changes.[23,24]

The most interesting finding of the Raman measurements concerns the features of the lattice phonon spectra of the TF form, which do not match those expected for a 3D triclinic crystal structure similar to the two bulk phases. The theoretical treatment of the lattice dynamics, together with the computation of the dispersion curves for the lattice modes, has allowed us to explain such features in terms of the 2D character of the TF form, shedding light on the actual nature of the films. As discussed in Sec. III E, this 2D character is somehow missed by the XRD technique, which probes different physical correlations. Altogether, Raman, AFM, and x-ray measurements provide a consistent picture of the differences between a 2D TF and a 3D bulk crystal.

II. METHODS

A. Experiment

Pentacene (Fluka) was used as received. The substrates consisted of silicon wafers with 2000 Å of thermal oxide and were cleaned by using acetone vapors before the deposition. Pentacene films were thermally deposited in high vacuum ($2 \cdot 10^{-8}$ mb) at two deposition rates, $\Phi_1 = 0.36 \pm 0.02$ Å/s and $\Phi_2 = 0.033 \pm 0.016$ Å/s, which was the lowest attainable rate. During the deposition, the substrate was at room temperature while the nominal film thickness D and the deposition rate Φ were monitored by a quartz-crystal microbalance (QCM) kept at 20° C. AFM (Smena; NT-MDT, Moscow) measurements were initially used to calibrate the QCM by measuring the coverage of sub-ML pentacene films. All films were investigated by AFM within the amplitude modulation technique (AM-AFM) under atmospheric conditions. The AFM topographic images were analyzed with the software Gwyddion.[25]

Raman spectra were obtained by placing the pentacene films on the stage of an optical microscope (Olympus BX40) interfaced to a Jobin Yvon T64000 Raman spectrometer, with 50× or 100× objectives, which allowed us to obtain a spatial resolution of about 1 μm and a theoretical field depth ranging from 7 to 25 μm. Spectra were recorded spanning the region 10–2000 cm^{-1}, with particular attention to the low-frequency region of the lattice phonons (10–150 cm^{-1}). The excitation wavelength was from a krypton laser tuned at 647.1 or 752.5 nm, providing sufficiently low energy to avoid strong background fluorescence from the sample in the low-wave-number region. The incoming power was reduced with neutral filters, with optical densities selected in each experiment to prevent sample damage. The actual power on the sample was always kept below 1 mW.

XRD measurements on the films were performed in specular geometry using a SmartLab-Rigaku diffractometer, equipped with a rotating anode ($\lambda Cu_{K\alpha} = 1.54180$ Å), followed by a parabolic mirror and a series of variable slits (placed before and after the sample).

B. Calculations

Harmonic phonon frequencies[26] were computed for the experimental TF structure,[10] using the potential model from a previous work,[27] which described quite well the experimental crystal structures and the phonon modes for both LT and HT phases. Given the structure, one computes the total potential energy V of the lattice and its second derivatives $\partial^2 V/\partial Q_{ma}\partial Q_{nb}$ with respect to all pairs of molecular coordinates Q_{ma} and Q_{nb}. Here $\boldsymbol{m}$ (or $\boldsymbol{n}$) is a lattice vector which indicates the position ($\boldsymbol{r}$ space) of the cell in the crystal, while a (or b) labels molecular coordinates within the cell. The dynamical matrix, given by the $\boldsymbol{r}$ space–to–$\boldsymbol{k}$ space (wave-vector) 3D Fourier transform of the potential derivatives, is numerically diagonalized, yielding the phonon frequencies ν_{ki} as a function of the wave vector $\boldsymbol{k}$ (dispersion curves). The label i distinguishes the various phonon branches, which are the different eigenvalues with the same $\boldsymbol{k}$.

III. RESULTS

A. Raman measurements

The Raman spectrum of a one-ML (nominal-thickness) film of pentacene deposited on SiO_2 with the higher growth rate $\Phi_1 = 0.36$ Å/s is shown in Fig. 1 for two selected wave-number intervals. The first interval spans the energy range of the lattice phonons; the second, that of the intramolecular C-H bending modes. The shape and position of these intramolecular bands are representative of each known bulk or TF structure of pentacene, as extensively described in the literature[28,29] and as shown in Fig. 3, so that the analysis of either energy interval allows for the structure identification.

As shown in Fig. 1, the bands of the intramolecular vibrations are easily detected even for the one-ML sample and readily assigned to the TF form. The intensity of the

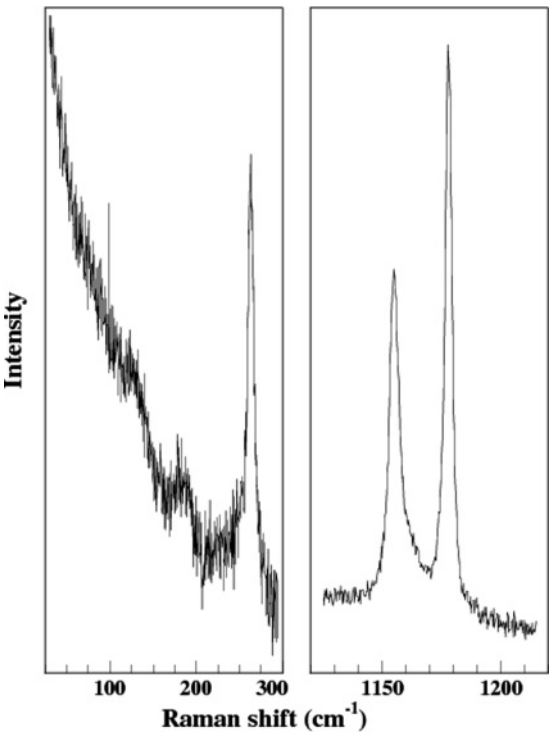

FIG. 1. Raman spectrum of one-ML film of pentacene on SiO_2 (growth rate Φ_1, $\lambda_{exc} = 647.1$ nm). Left: Lattice phonon region. Right: Region of C-H bending modes.

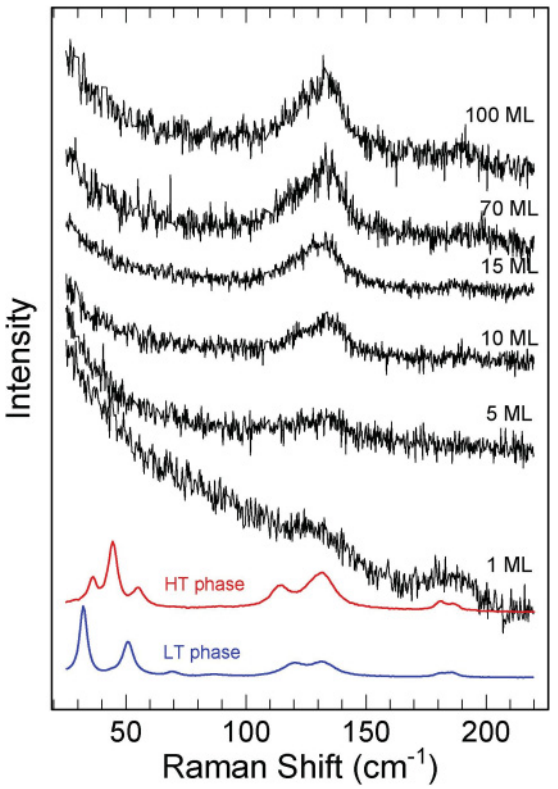

FIG. 2. (Color online) Lattice phonon Raman spectra of pentacene films on SiO_2 (growth rate Φ_1, $\lambda_{exc} = 752.5$ nm) with a nominal thickness varying from 1 to 100 MLs. Spectra of the two known bulk crystal phases LT and HT are also reported as a reference.

intramolecular Raman modes is, indeed, exceptionally high compared to that of other compounds such as, for instance, α-sexithiophene.[30] The lattice phonons in the low-energy region, instead, are ill defined and very weak, as it clearly appears when their intensities are compared to those of the intramolecular vibrations. The best probe for this is provided by the intramolecular mode lying at 263 cm^{-1}, shown in the left panel in Fig. 1. In the bulk, depending on the crystal orientation, this mode displays an intensity 1.5 to 4 times lower than that of the lattice phonons around 130 cm^{-1},[31] whereas here it is found to dominate the low-energy spectrum. The weakness of the signal of lattice phonon modes in a one-ML-thick sample is somehow unexpected, in light of the intensity of the intramolecular vibrations, and more interestingly, no significant intensification is observed upon increasing the film thickness D. This is shown in Fig. 2, where the spectra of a series of films of variable D are shown, together with the reference spectra[32] of the two known bulk phases. The spectra of the intramolecular vibrations, not reported here, match that shown in Fig. 1 and thus indicate that these films all belong to the TF form.

The lattice phonon spectra of the two bulk forms can be conveniently analyzed by separating the six $\boldsymbol{k} = 0$ lattice modes predicted by the factor-group analysis into two spectral regions: (i) the region below 100 cm^{-1}, which shows the strongest bands with a pattern typical of each polymorph, and therefore represents the fingerprint of the structure; (ii) the broad features around 130 cm^{-1}, very similar for both polymorphs. In the films the lower frequency bands are always missing, regardless of the number of layers, while the broad phonon pattern at higher wave numbers, albeit weak, is always detected and resembles that observed for the bulk forms. On the basis of the known packing and symmetry of the TF

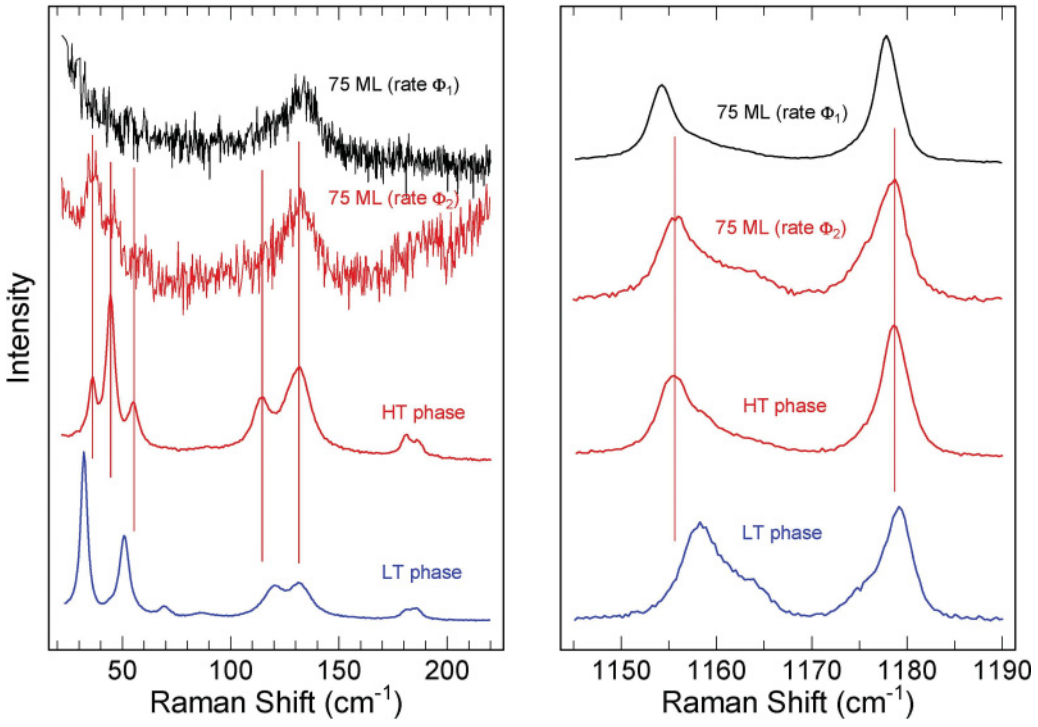

FIG. 3. (Color online) Raman spectra of pentacene films on SiO_2, at growth rates Φ_1 and Φ_2 ($\lambda_{exc} = 752.5$ nm): lattice phonon (left) and C-H bending region (right). Spectra of bulk crystal phases are also reported.

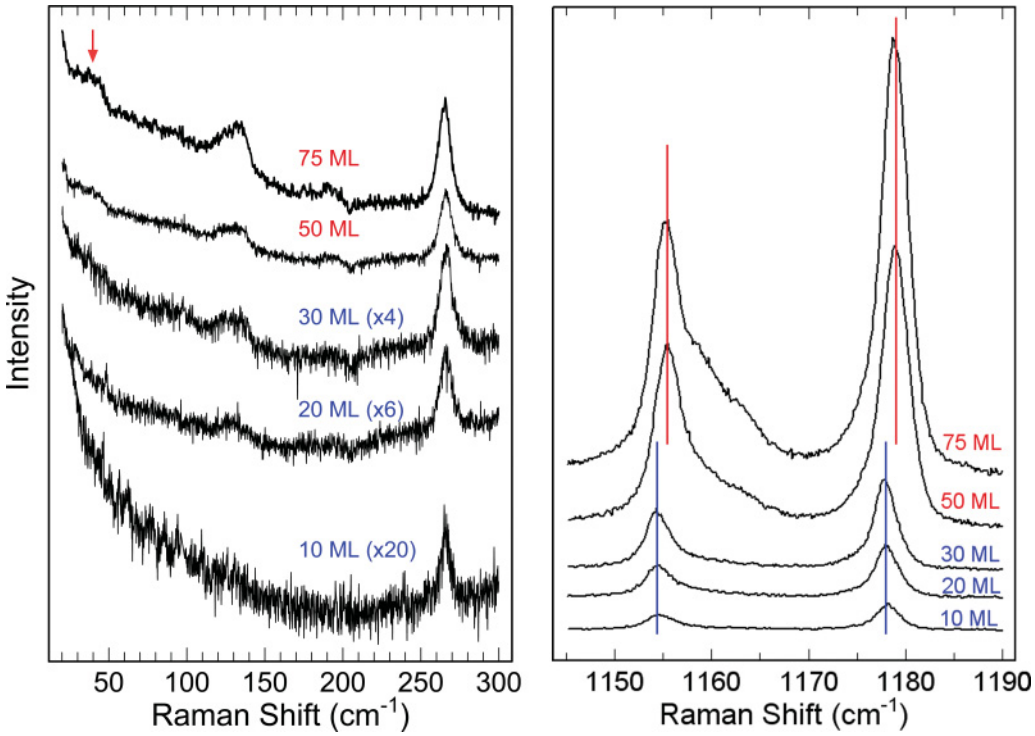

FIG. 4. (Color online) Raman spectra of pentacene films grown on SiO_2 at rate Φ_2 ($\lambda_{exc} = 752.5$ nm): lattice phonon (left) and C-H bending region (right). Nominal sample thickness is indicated.

structure,[10] the low-frequency phonons should be observed. The reason why this does not happen must be linked to some structural characteristics affecting the dynamics, as shown in Sec. III D.

A qualitative analysis of the intensities of the high-frequency lattice bands in Fig. 2, relative to those of the intramolecular modes, indicates that they do not change significantly with the numbers of layers in the films. The intensities carry information on the degree of crystallinity: the higher the long-range order, the stronger should be the lattice phonon signal which probes it. Increasing the thickness of our samples, therefore, does not enhance their crystallinity, viewed as a measure of the 3D order.

To increase the crystallinity of the TF form or, equivalently, its 3D order, we therefore decided to reduce the growth rate to $\Phi_2 = 0.033$ Å/s, one order of magnitude below Φ_1. The spectra of samples 75 MLs thick, recorded at rates Φ_1 and Φ_2, are shown in Fig. 3, together with the spectra[32] of the bulk phases. We see immediately that a fully developed phonon pattern at low frequencies, indicative of a 3D film, starts to appear once the rate is lowered to Φ_2. Rather surprisingly, this phonon pattern cannot be ascribed to the TF structure but, instead, matches that of the HT bulk phase. The assignment to HT phase is further confirmed by the characteristic frequencies of the bending modes above 1150 cm^{-1} (right panel of Fig. 3) and by the XRD measurements discussed in Sec. III C.

A collection of spectra recorded at rate Φ_2, for a series of films of variable nominal thickness D, are shown in Fig. 4. We see immediately that the just-mentioned phonon pattern only appears once D exceeds 30 MLs (Fig. 4, left). The bending frequencies characteristic of the HT phase (Fig. 4, right) are also revealed only above 30 MLs.

As anticipated in Sec. I, the occurrence of the HT phase was expected. In fact, this phase is found in films at varying thicknesses and depending on the choice of the growth conditions.[6,9,14,16] What is remarkable is that a full lattice phonon pattern attributable to the TF form is never observed, not even in samples where this form is certainly present.

B. AFM measurements

AM-AFM[33] topographic images of pentacene films grown at the two deposition rates Φ_1 and Φ_2 are shown in Fig. 5. As discussed in the literature,[33–35] these apparently irregular films are self-affine (i.e., present a similar morphology upon rescaling of their vertical or horizontal dimensions) and can be analyzed in terms of scaling exponents which describe the dependence of the fluctuations of the film height $h(x,y)$ on the nominal film thickness D and on the lateral length scale R. These exponents, which unambiguously distinguish among the various growth mechanisms proposed in theoretical works,[20,36,37] are defined in terms of appropriate statistical descriptors, which we have obtained by analyzing the image morphology with the software Gwyddion.[25]

The simplest of these descriptors, shown in Fig. 6(a), is the rms roughness σ, which is the standard deviation $\sigma = \langle (h - \langle h \rangle)^2 \rangle$ of the film height h. The roughness σ evolves with the film thickness D with a power law $\sigma \propto D^{\beta}$, where β is the growth exponent. A closely related descriptor, shown in Fig. 6(b), is the height difference correlation function (HDCF),[34] which is the mean square height difference $g(R) = \langle [h(x,y) - h(x',y')]^2 \rangle$ between pairs of points laterally separated by a distance $R = \sqrt{(x-x')^2 + (y-y')^2}$. The HDCF displays distinct behaviors for $R \ll \xi$ and $R \gg \xi$, where ξ is

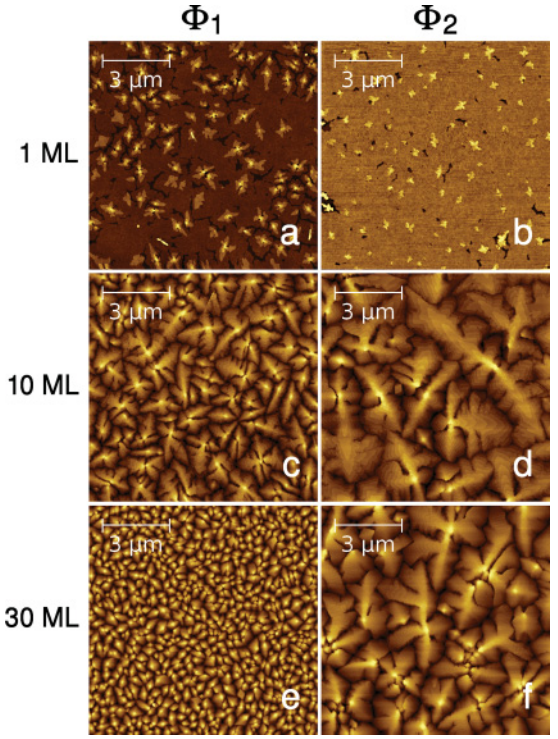

FIG. 5. (Color online) Topographic images of pentacene films deposited on SiO_2 at room temperature with rates Φ_1 and Φ_2 for increasing nominal thickness D: 1, 10, and 30 MLs.

the correlation length. For $R \ll \xi$ one expects a power law increase $g(R) \propto R^{2\alpha}$ where α is the roughness exponent. For $R \gg \xi$ the heights become uncorrelated and $g(R)$ saturates at $2\sigma^2$ [see Fig. 6(b)]. Assuming that the regimes $R \ll \xi$ and $R \gg \xi$ are connected through a scaling form $g(R) = 2\sigma^2 \tilde{g}(R/\xi)$, it follows that the scaling exponents are related by $\beta = \alpha/z + \lambda$, where z is the dynamic exponent and λ is the steepening exponent representing the surface slope. For $\lambda = 0$ (no steepening) one has $\beta = \alpha/z$. Scaling with $\lambda > 0$ is referred to as anomalous.[38]

For both selected deposition rates, pentacene films one or two layers thick grow layer by layer[39] and thus exhibit a smooth surface [Figs. 5(a) and 5(b)]. After the second ML, the surface roughness σ begins to increase [Fig. 6(a)] with the expected[34] power law D^β, until it reaches a saturation value σ_{sat}. The roughness at 2 MLs, $\sigma = 8 \pm 3$ Å, is independent of the deposition rate. For the higher rate Φ_1, we find a growth exponent $\beta = 0.35 \pm 0.02$ and a saturated surface roughness $\sigma_{sat} = 86 \pm 3$ Å, which is reached for the critical thickness $D_{sat} = 16 \pm 1$ MLs. These parameters increase to $\beta = 0.75 \pm 0.11$ and $\sigma_{sat} = 104 \pm 3$ Å when the deposition rate is decreased to Φ_2, while D_{sat} decreases to 11 ± 1 MLs, in agreement with the β increase.

These two different β values correspond to two different film morphologies and, indeed, to two different growth mechanisms (see Fig. 5). The lower β value corresponds to the random deposition (RD) scenario ($\beta \leqslant \beta_{RD} = 0.5$), which applies to a molecular system where mass transport between layers of the growing film is inhibited[37] by molecular step edge barriers.[40] Since mass transport processes along the growing surface are driven by differences in bonding energy, organic

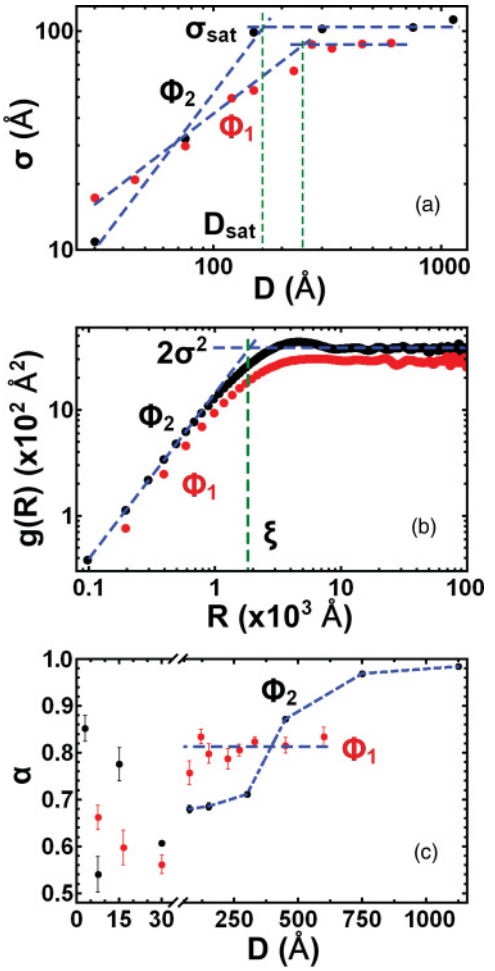

FIG. 6. (Color online) Statistical descriptors extracted from the topographic images, for deposition rates Φ_1 and Φ_2. (a) σ vs D on log-log scale. Dashed lines indicate the thickness D_{sat} where σ saturates. The slopes of the straight lines before D_{sat} are the β exponents. (b) $g(R)$ vs R on log-log scale (HDCF plots). The dashed line in the correlated part of $g(R)$ (below the correlation length ξ) has slope 2α. Above ξ, the heights become uncorrelated and $g(R)$ saturates to $2\sigma^2$. (c) α vs D.

films grown in the RD limit will generally tend to be smooth, i.e., they show 2D layer-by-layer growth, as predicted[20] for pentacene at deposition rate Φ_1. The larger β value, instead, corresponds to 3D growth, as predicted[20] at rate Φ_2.

The roughness exponent α as a function of the nominal film thickness D, obtained at rates Φ_1 and Φ_2 by analyzing topographic images 10×10 μm, is shown in Fig. 6(b). For films grown at rate Φ_1, the roughness exponent α shows two distinct behaviors for the first two layers and higher thicknesses, respectively. The former shows α values following the layer-by-layer growth of the first two MLs (higher and lower α values are observed for sub-ML and ML films). For higher thicknesses, α jumps to the constant value 0.81 ± 0.03 [Fig. 6(c)]. As theoretically predicted[36] and experimentally observed for similar molecules,[33] this α value is typical of molecular films composed of pyramids ($\alpha = 0.83$) grown by molecular beam epitaxy (MBE) in the kinetic roughening framework. When the rate is decreased to Φ_2, the roughness exponent for the first two MLs mimics the oscillating behavior

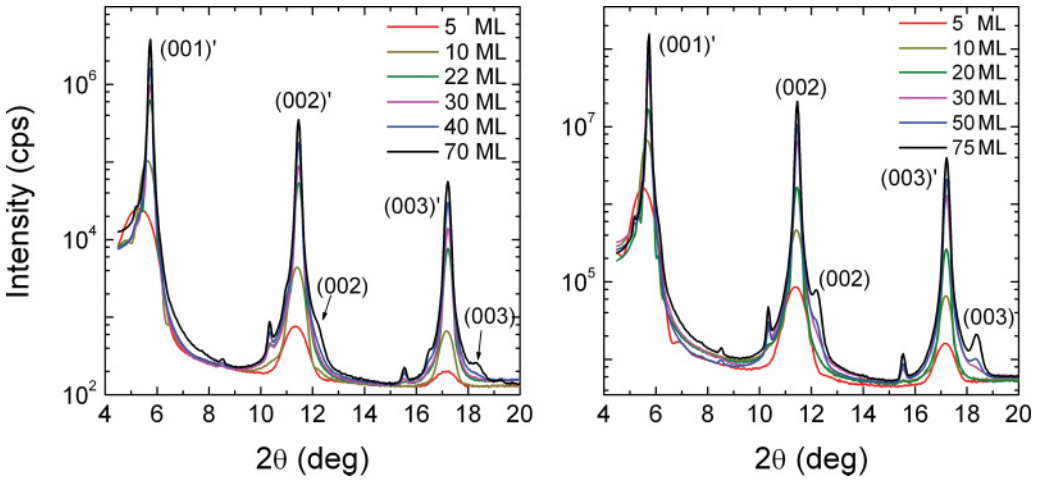

FIG. 7. (Color online) Specular XRD patterns of pentacene films grown on SiO_2 at rates Φ_1 (left) and Φ_2 (right).

observed for higher rate. From the second ML, it increases monotonically with increasing thickness, from 0.680 ± 0.008 to 0.984 ± 0.003 [Fig. 6(c)]. As observed elsewhere,[20,33,35] this trend suggests an evolution of the surface morphology toward 3D growth, and in particular, it can be explained in terms of the pyramid formation framework.[36] The deposition rate can be used as the experimental parameter to distinguish between kinetic roughening and pyramid formation frameworks, although they are very similar. In addition, the α value close to 1 (within the confidence interval) for the thicker film corresponds to the super-roughening limit.[41] This limit is corroborated by the previously mentioned β value, which collocates pentacene films grown at Φ_2 within the rapid-roughening scenario.[37,42]

The dynamic exponent z is the last statistical descriptor used to identify the scaling behavior of pentacene films for the two deposition rates. It describes how the correlation length ξ evolves with the film thickness D through the power law $\xi \propto D^{1/z}$. At rate Φ_1 the correlation length ξ ranges from ≈140 to ≈230 nm for increasing D, with $1/z = 0.25 \pm 0.05$. When the rate is lowered to Φ_2, $1/z$ decreases to 0.12 ± 0.03. Both rates, Φ_1 and Φ_2, show an anomalous growth behavior, with $\lambda = 0.15 \pm 0.07$ and $\lambda = 0.7 \pm 0.1$, respectively. These results confirm 3D growth for the low rate Φ_2 (pyramids with higher slopes lead to rougher surfaces) and 2D growth for the high rate Φ_1 (pyramids with lower slopes lead to smoother surfaces).

C. XRD measurements

The structure of the various films grown at rates Φ_1 and Φ_2, with nominal thickness D from 5 to 75 MLs, has been characterized by XRD to confirm the occurrence of TF and HT structures. Analysis of the specular XRD patterns (Fig. 7) indicates that all the films are polycrystalline with the typical fiber-like texturing, i.e., with the *ab* layers parallel to the substrate surface.[10] The thinner films (up to 30 MLs) consist only of the TF form, whose reflections are marked by primes in the Fig. 7. The TF and HT bulk forms coexist in the thicker films, in agreement with the Raman results discussed in Sec. III A. To evaluate the amount of the two forms, we have analyzed the reflections (003) and (003)′, because of their lower overlap.

The position of the peaks yields $d(001)$ layer spacings which, in agreement with the literature,[5,10,11,16] are 14.5 and 15.4 Å for the HT and TF forms, respectively. The FWHM of the peaks instead gives the coherent domain lengths perpendicular to the surface, $L_\perp^{HT}$ and $L_\perp^{TF}$ for the bulk and film forms, respectively. The lengths, reported in Table I, are affected by statistical fit errors, which reach 100 Å for the HT phase, whose peaks are weak and wide, and are about 1.5 Å for the TF form. Once divided by the appropriate $d(001)$ spacings, the lengths give the corresponding coherent thicknesses $D_\perp^{HT}$ and $D_\perp^{TF}$ (expressed in MLs and also reported in Table I).

TABLE I. Structural parameters of pentacene TFs grown at rates $\Phi_1 = 0.36$ Å/s and $\Phi_2 = 0.033$ Å/s, extracted by XRD analysis. Statistical errors are 1.5 Å (0.1 ML) for the TF form and 100 Å (7 ML) for the HT phase.

Deposition rate Φ_1					Deposition rate Φ_2				
D (ML)	$L_\perp^{TF}$ (Å)	$D_\perp^{TF}$ (ML)	$L_\perp^{HT}$ (Å)	$D_\perp^{HT}$ (ML)	D (ML)	$L_\perp^{TF}$ (Å)	$D_\perp^{TF}$ (ML)	$L_\perp^{HT}$ (Å)	$D_\perp^{HT}$ (ML)
5	109	7.0			5	126	8.1		
10	173	11.2			10	205	13.2		
22	285	18.5			20	336	21.7		
30	339	22.0			30	442	28.5		
40	388	25.2			50	516	33.3	300	21
70	425	27.6	175	12	75	558	36.2	315	22

For thinner films (up to 30 MLs), $D_{\perp}^{\mathrm{TF}}$ almost attains the nominal thickness D. For thicker films $D_{\perp}^{\mathrm{TF}}$ reaches a saturation value above 30 MLs, while $D_{\perp}^{\mathrm{HT}}$ does not make up for the difference. This was expected,[21] since only under the hypothesis that the system consists of a lower TF bed with a uniform HT cover would $D_{\perp}^{\mathrm{TF}}$ and $D_{\perp}^{\mathrm{HT}}$ add up to D. Clearly, this simplified picture does not describe the actual distribution of HT crystallites,[21,43] which exhibit a nonuniform distribution and, thus, do not scatter in-phase in the specular directions,[21] leading to an apparent underestimation of the HT phase thickness. It may be noted that the $D_{\perp}^{\mathrm{TF}}$ apparent saturation thickness at rate Φ_1 ($\approx$28 MLs) is significantly lower than at Φ_2 ($\gtrsim$36 MLs). This indicates that, as expected, samples grown at rate Φ_2 are more ordered.

D. Calculations

Lattice dynamics calculations provide the key to understanding the Raman spectra of TF pentacene in connection with its molecular packing. The six $\boldsymbol{k} = 0$ Raman active lattice phonons (g symmetry) computed for rigid molecules are purely librational in character, since all molecules lie on the crystal inversion centers. They also follow the expected pattern of *decreasing* frequencies $\nu_L > \nu_M > \nu_N$, where L, M, and N, in order of *increasing* moment of inertia, indicate librations around the long-in-plane, short-in-plane, and normal-to-plane molecular axes. The spectroscopic observations discussed in Sec. III A can be summarized by stating that the high-frequency ν_L modes are observed almost unchanged in the LT, HT, and TF structures, whereas the low-frequency modes differ in the LT and HT phase and vanish altogether in the TF form. This difference between the ν_L modes and the ν_M or ν_N modes must be related to some regularity in the molecular packing of all pentacene forms.

The unit cell (direct lattice) of the TF structure[10] is shown in Fig. 8. As in the LT and HT polymorphs, the TF triclinic unit cell contains two inequivalent molecules, situated at the (0,0,0) and ($\frac{1}{2}$,$\frac{1}{2}$,0) positions on the ab layer plane and standing approximately normal to the plane. The various structures mainly differ in the angle between the pentacene molecules and the layer planes and in the details of the herringbone arrangement. Intralayer nearest neighbors occur at direct lattice vectors $(\boldsymbol{a} \pm \boldsymbol{b})/2$, while interlayer neighbors occur at much longer vectors $\boldsymbol{c}$.

As is well known,[26] optical spectroscopy yields the frequencies ν_i of the lattice modes for the wave vector $\boldsymbol{k} = (0,0,0)$, that is, under conditions in which all the unit cells of the crystal move in phase. For this reason, it is the dependence of the vibrational frequencies ν_{ki} on the wave vector $\boldsymbol{k}$ (i.e., the dispersion curves) which encodes most information on the interactions between molecules in different crystal cells. This information, which can be extracted by analyzing the phonon dispersion curves for the infinite crystal, carries over to finite crystals, allowing us to rationalize the spectra in terms of the directionality and dimensionality of the intermolecular interactions. The Brillouin zone (reciprocal lattice) for the TF structure[10] and dispersion curves for the Raman active modes calculated for wave vectors $\boldsymbol{k}$ along the reciprocal lattice directions $(k,k,0)$, $(k,-k,0)$, and $(0,0,k)$ are shown in Fig. 8. The axis $\boldsymbol{c}^*$ of the reciprocal lattice is normal to the

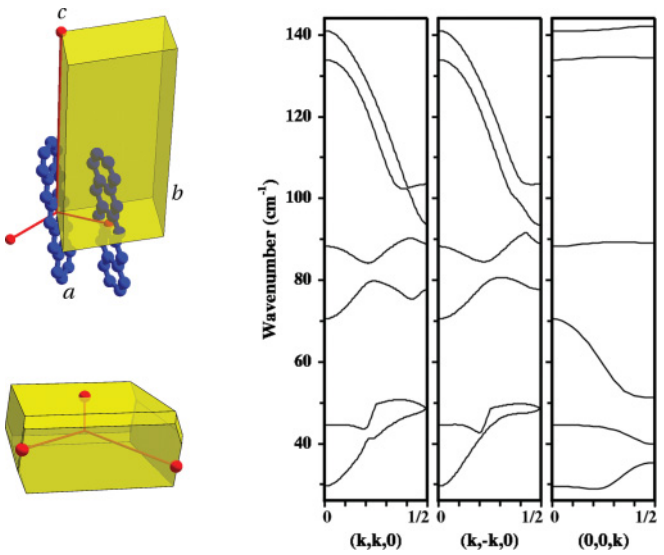

FIG. 8. (Color online) Top left: Unit cell of TF pentacene.[10] The three pins at direct lattice vectors $(\boldsymbol{a} \pm \boldsymbol{b})/2$ and $\boldsymbol{c}$ indicate the intralayer and interlayer nearest neighbors. Bottom left: Brillouin zone. The three pins are at reciprocal lattice vectors $(\boldsymbol{a}^* \pm \boldsymbol{b}^*)/2$ and $\boldsymbol{c}^*/2$. Right: Calculated dispersion curves for Raman active lattice phonons along the directions $(k, \pm k,0)$ and $(0,0,k)$.

ab layer planes, i.e., is normal to the substrate. The phonon dispersion calculated for wave vectors $\boldsymbol{k} = (0,0,k)$ along $\boldsymbol{c}^*$ thus probes the interactions between different layers. The dispersion calculated for vectors $\boldsymbol{k} = (k, \pm k,0)$ along $\boldsymbol{a}^* \pm \boldsymbol{b}^*$ instead probes the intralayer interactions.

It can be seen that all modes exhibit large dispersion in the $\boldsymbol{k} = (k, \pm k,0)$ directions (within the layer), whereas only low-frequency modes below 80 cm^{-1} present dispersion in the $\boldsymbol{k} = (0,0,k)$ direction (perpendicular to the layer). This indicates that intralayer interactions are always significant, whereas interlayer interactions affect low-frequency modes only. This difference can be rationalized by noting that high-frequency ν_L modes represent librations around the long-in-plane molecular axes, which are almost perpendicular to the ab layers. This kind of motion has only a minor effect on molecule-molecule and atom-atom distances between different layers, but a larger effect on intralayer distances. This is especially true because, as already mentioned, intralayer nearest-neighbor distances are much shorter than interlayer ones. High-frequency modes are largely 2D in character, while low-frequency modes are 3D. This distinction may be made even more clear by noting that for wave vectors at the boundary $\boldsymbol{k} = \boldsymbol{c}^*/2 = (0,0,1/2)$ of the Brillouin zone, cells on adjacent ab layers move with opposite phases. Modes insensitive to the relative motion of molecules in adjacent layers, or, equivalently, modes weakly affected by the interactions between layers, will thus exhibit negligible dispersion. Modes with large dispersion, on the contrary, necessarily involve strong interactions between different unit cells. While all phonon modes are certainly observable in a 3D crystal, we expect that highly dispersed modes involving strong interactions between different ab layers will be progressively washed out for increasingly thin films or, equivalently, for vertically disordered samples which lack spatial correlation in the direction normal to the substrate. The 2D ν_L modes

with negligible dispersion along $\boldsymbol{c}^*$, instead, should be more resilient and could even be observable for MLs or for disordered multilayer systems.

E. Discussion and conclusion

Confocal micro Raman spectroscopy, AFM, and XRD, supported by lattice dynamics calculations, have been used to investigate pentacene films obtained by vacuum deposition on SiO_2 substrates. We have found that the high sensitivity of the micro Raman experimental setup allows us to distinguish between TF and bulk crystal phases *even for one-ML samples*. While XRD and Raman are both effective tools for determining the phase of a material, one has to keep in mind that the determination is based on different physical properties. In any case, confocal micro-Raman spectroscopy once again proves to be a fast and reliable diagnostic tool for *in situ* characterization of the phase identity,[24] The calculated phonon dispersion curves provide the key to the interpretation of the TF lattice phonon Raman spectrum, showing that their characteristic spectra originate from a loss of spatial correlation along the axis $\boldsymbol{c}^*$ normal to the SiO_2 substrate. The calculations, in fact, show that different phonon modes probe intermolecular interactions along different directions. By analyzing the Raman spectra we find that modes involving interlayer interactions are never observable in TF structures, regardless of the sample thickness, while they are always observable in bulk forms. Modes involving intralayer interactions are instead always observable for both bulk and TF forms. Thus, we may safely conclude that the TF form is intrinsically a 2D structure, in which dynamical correlations between different layers are weak or nonexistent.

Pentacene films on amorphous SiO_2, with increasing nominal thickness D, were grown at two different deposition rates, $\Phi_1 = 0.36$ Å/s and $\Phi_2 = 0.033$ Å/s. For the higher deposition rate Φ_1, regardless of the thickness, the Raman data indicate that film growth occurs in the TF form. The 2D nature of this form is compatible with a layer-by-layer growth model in which the layers are stacked one on top of the other without necessarily building up a genuine 3D ordered structure. When the deposition rate is lowered to Φ_2, growth of the TF form initially takes place, followed, for sufficiently thick films, by the HT bulk phase. Decreasing the growth rate thus induces order, as expected, and the 2D dynamic behavior of the system changes into that of a 3D system. The simultaneous occurrence of HT and TF forms in pentacene films is widely documented in the literature,[6,7,9,11,14,16] and the transformation from TF to HT structure may take place either upon exposure of the film to solvent vapors[44] or upon thermal annealing.[7] These experimental findings clearly suggest that the TF structure is thermodynamically unstable with respect to the HT structure. Previous calculations[20,45] have indeed proved that the TF structure does not correspond to a stable energy minimum and spontaneously transforms into the HT structure.

The analysis of the AFM images of the various samples indicates that the 2D or 3D dynamics revealed by the Raman results actually corresponds to two different growth mechanisms. As predicted by the theory,[20] films formed at the higher deposition rate Φ_1 exhibit quasi-layer-by-layer growth,[37] yielding rather smooth continuous films suitable for charge transport. Films formed at the lower rate Φ_2 exhibit a 3D growth[20] according to the rapid roughening scenario,[37,42] leading to ill-connected grains.

The XRD measurements unambiguously confirm that only the TF form is present in the thinner films, at least up to 30 MLs, whereas the TF and HT bulk forms coexist in thicker films. We were initially puzzled by the observation that, for sufficiently thin films, the coherent domain lengths perpendicular to the surface $D_{\perp}^{\mathrm{TF}}$ coincide with the nominal thickness D, apparently indicating that the crystalline domains of the TF form extend continuously through the film thickness, without any significant lack of *vertical* periodicity. This seems to imply that TF systems exhibit a 3D crystalline order, at variance with the Raman observations. The contradiction, however, is not genuine, since specular XRD is sensitive to the spacing between the *ab* layers but not to the order within each layer. An arrangement like that in turbostratic graphene,[46] where successive 2D layer planes have slipped out of alignment, would exhibit a specular XRD pattern indistinguishable from that of a fully ordered 3D crystalline structure. As anticipated above, in fact, Raman and specular XRD experiments probe different kinds of interlayer correlations.

It is common opinion[20,47] that in organic semiconductors, irrespective of the substrate, a 3D structure begins to appear after a few MLs, five or six at most. If this opinion is correct, pentacene films grown on SiO_2 constitutes an exceptional case. At rate Φ_1 a 3D structure is never revealed by the Raman spectra (at least up to 100 MLs), and even at the lower rate Φ_2 more than 30 MLs are needed before a 3D structure starts to appear. The change of form, from TF to bulk phase, is thus mainly driven by different growth conditions, rather than by the thickness of the film, that is, by the distance from a structure-inducing surface. Recent MD simulations on pentacene monolayers and thin films,[48] in fact, indicate that deposition history, rather than interaction with the substrate, controls the film structure. This finding may have important consequences for the preparation of pentacene devices with good charge transport properties.

ACKNOWLEDGMENTS

The research leading to these results received funding from the European Community's Seventh Framework Programme (FP7/2007-2013) under Grant Agreement No. 212311 of the ONE-P project. We also acknowledge the skillful assistance of Dr. Massimo Placidi, Horiba Jobin Yvon srl.

*aldo.brillante@unibo.it

[1] C. D. Dimitrakopoulos and P. R. L. Malenfant, Adv. Mater. **14**, 99 (2002).

[2] R. B. Campbell, J. M. Roberston, and J. Trotter, Acta Crystallogr. **15**, 289 (1962).

[3] D. Holmes, S. Kumaraswamy, A. J. Matzger, and K. P. Vollhardt, Chem. Eur. J. **5**, 3399 (1999).

[4] T. Siegrist, C. Besnard, S. Haas, M. Schiltz, P. Pattison, D. Chernyshov, B. Batlogg, and C. Kloc, Adv. Mater. **19**, 2079 (2007).

[5]C. C. Mattheus, A. B. Dros, J. Baas, A. Meetsma, J. L. de Boer, and T. T. M. Palstra, Acta Crystallogr. Sec. C **57**, 939 (2001).
[6]I. P. M. Bouchoms, W. A. Schoonveld, J. Vrijmoeth, and T. M. Klapwijk, Synth. Met. **104**, 175 (1999).
[7]C. C. Mattheus, A. B. Dros, J. Baas, G. T. Oostergetel, A. Meetsma, J. L. de Boer, and T. T. M. Palstra, Synth. Met. **138**, 475 (2003).
[8]S. E. Fritz, S. M. Martin, C. D. Frisbie, M. D. Ward, and M. F. Toney, J. Am. Chem. Soc. **126**, 4084 (2004).
[9]R. Ruiz, D. Choudhary, B. Nickel, T. Toccoli, K. C. Chang, A. C. Mayer, P. Clancy, J. M. Blakely, R. L. Headrick, S. Iannotta, and G. G. Malliaras, Chem. Mater. **16**, 4497 (2004).
[10]S. Schiefer, M. Huth, A. Dobrinevski, and B. Nickel, J. Am. Chem. Soc. **129**, 10316 (2007).
[11]H. Yoshida, K. Inaba, and N. Sato, Appl. Phys. Lett. **90**, 181930 (2007).
[12]D. Nabok, P. Puschnig, C. Ambrosch-Draxl, O. Werzer, R. Resel, and D.-M. Smilgies, Phys. Rev. B **76**, 235322 (2007).
[13]T. Siegrist, Ch. Kloc, J. H. Schön, B. Batlogg, R. C. Haddon, S. Berg, and G. A. Thomas, Angew. Chem., Int. Ed. Engl. **40**, 1732 (2001).
[14]H. Yoshida and N. Sato, Appl. Phys. Lett. **89**, 101919 (2006).
[15]J. S. Wu and J. C. H. Spence, J. Appl. Crystallogr. **37**, 78 (2004).
[16]T. Kakudate, N. Yoshimoto, and Y. Saito, Appl. Phys. Lett. **90**, 081903 (2007).
[17]R. Ruiz, A. C. Mayer, G. G. Malliaras, B. Nickel, G. Scoles, A. Kazimirov, H. Kim, R. L. Headrick, and Z. Islam, Appl. Phys. Lett. **85**, 4926 (2004).
[18]We define a monolayer (ML) as a layer of ordered and packed molecules orthogonal to the surface and that completely covers it. A nominal ML is equivalent to 15 Å of pentacene molecules deposited on the SiO_2 substrate.
[19]J. E. Northrup, M. L. Tiago, and S. G. Louie, Phys. Rev. B **66**, 121404 (2002).
[20]S. Verlaak, S. Steudel, P. Heremans, D. Janssen, and M. S. Deleuze, Phys. Rev. B **68**, 195409 (2003).
[21]A. C. Mayer, A. Kazimirov, and G. G. Malliaras, Phys. Rev. Lett. **97**, 105503 (2006).
[22]A. Shehu, S. D. Quiroga, P. D'Angelo, C. Albonetti, F. Borgatti, M. Murgia, A. Scorzoni, P. Stoliar, and F. Biscarini, Phys. Rev. Lett. **104**, 246602 (2010).
[23]A. Brillante, I. Bilotti, R. G. Della Valle, E. Venuti, M. Masino, and A. Girlando, Adv. Mater. **17**, 2549 (2005).
[24]A. Brillante, I. Bilotti, R. G. Della Valle, E. Venuti, and A. Girlando, CrystEngComm. **10**, 937 (2008).
[25]D. Neas and P. Klapetek, Gwyddion free software; available at: [http://gwyddion.net/].
[26]M. Born and K. Huang, *Dynamical Theory of Crystal Lattices* (Oxford University Press, New York, 1954).
[27]R. G. Della Valle, E. Venuti, L. Farina, A. Brillante, M. Masino, and A. Girlando, J. Phys. Chem. B **108**, 1822 (2004).
[28]A. Brillante, R. G. Della Valle, L. Farina, A. Girlando, M. Masino, and E. Venuti, Chem. Phys. Lett. **357**, 32 (2002).
[29]R. He, I. Dujovne, L. Chen, Q. Miao, C. F. Hirjibehedin, A. Pinczuk, C. Nuckolls, C. Kloc, and A. Ron, Appl. Phys. Lett. **84**, 987 (2004).
[30]A. Brillante, I. Bilotti, C. Albonetti, J.-F. Moulin, P. Stoliar, F. Biscarini, and D. M. de Leeuw, Adv. Funct. Mater. **17**, 3119 (2007).
[31]L. Farina, K. Syassen, A. Brillante, R. G. Della Valle, E. Venuti, and N. Karl, High Press. Res. **23**, 349 (2003).
[32]E. Venuti, R. G. Della Valle, A. Brillante, M. Masino, and A. Girlando, J. Am. Chem. Soc. **124**, 2128 (2002).
[33]F. Biscarini, P. Samori, O. Greco, and R. Zamboni, Phys. Rev. Lett. **78**, 2389 (1997).
[34]F. Schreiber, Phys. Status Solidi A **201**, 1037 (2004).
[35]P. Viville, R. Lazzaroni, J. L. Brèdas, P. Moretti, P. Samorí, and F. Biscarini, Adv. Mater. **10**, 57 (1998).
[36]M. Siegert and M. Plischke, Phys. Rev. E **53**, 307 (1996).
[37]J. Krug, Physica A **340**, 647 (2004).
[38]J. Krug, Phys. Rev. Lett. **75**, 1795 (1995).
[39]A. C. Mayer, R. Ruiz, H. Zhou, R. L. Headrick, A. Kazimirov, and G. G. Malliaras, Phys. Rev. B **73**, 205307 (2006).
[40]R. L. Schwoebel and E. J. Shipsey, J. Appl. Phys. **37**, 3682 (1966).
[41]S. Das Sarma, S. V. Ghaisas, and J. M. Kim, Phys. Rev. E **49**, 122 (1994).
[42]A. C. Dürr, F. Schreiber, K. A. Ritley, V. Kruppa, J. Krug, H. Dosch, and B. Struth, Phys. Rev. Lett. **90**, 016104 (2003).
[43]H. L. Cheng, Y. S. Mai, W. Y. Chou, L. R. Chang, and X. W. Liang, Adv. Funct. Mater. **17**, 3639 (2007).
[44]D. J. Gundlach, T. N. Jackson, D. G. Schlom, and S. F. Nelson, Appl. Phys. Lett. **74**, 3302 (1999).
[45]R. G. Della Valle, E. Venuti, A. Brillante, and A. Girlando, Chem. Phys. Chem. **10**, 1783 (2009).
[46]D. R. Lenski and M. S. Fuhrer, J. Appl. Phys. **110**, 013720 (2011).
[47]J.-F. Moulin, F. Dinelli, M. Massi, C. Albonetti, R. Kshirsagar, and F. Biscarini, Nucl. Instrum. Methods Phys. Res. Sec. B **246**, 122 (2006).
[48]M. Yoneya, M. Kawasaki, and M. Ando, J. Phys. Chem. C **116**, 791 (2012).